Electrochimica Acta 368 (2021) 137552

Contents lists available at ScienceDirect

Electrochimica Acta

journal homepage: www.elsevier.com/locate/electacta

Synthesis and characteristics of novel TPA-containing electrochromic poly(ether sulfone)s with dimethylamino substituents

Chiao-Ling Huang [a], Yu-Ruei Kung [b], Yu-Jen Shao [a], Guey-Sheng Liou [a,c,*]

[a] Institute of Polymer Science and Engineering, National Taiwan University, No.1, Sec. 4, Roosevelt Rd., Taipei 10617, Taiwan
[b] Department of Chemical Engineering and Biotechnology, Tatung University, No.40, Sec. 3, Zhongshan N. Rd., Taipei 10452, Taiwan
[c] Advanced Research Center for Green Materials Science and Technology, National Taiwan University, Taipei 10617, Taiwan

ARTICLE INFO

Article history:
Received 19 October 2020
Revised 21 November 2020
Accepted 23 November 2020
Available online 2 December 2020

Keywords:
Electrochromism
Triphenylamine
Dimethylamino group
Poly(ether sulfone)s
Silyl method

ABSTRACT

Newly designed dimethylamine-substituted triphenylamine (TPA) derivatives, *N,N'*-(1,4-phenylene)bis(*N*-(4-((*tert*-butyldimethylsilyl)oxy)phenyl)-*N",N"*-dimethylbenzene-1,4-diamine) (**NTPPA-2Si**) and *N,N'*-((1,1′-biphenyl)-4,4′-diyl)bis(*N*-(4-((*tert*-butyldimethylsilyl)oxy)phenyl)-*N",N"*-dimethylbenzene-1,4-diamine) (**NTPB-2Si**), with silyl ether protecting groups were readily synthesized. Subsequently, novel electroactive aromatic poly(ether sulfone)s (PES), **NTPPA-PES** and **NTPB-PES**, could be obtained from silyl polycondensation. The PESs were readily soluble in commonly used laboratory organic solvents and could be solution-cast into tough and amorphous films with moderate levels of glass-transition temperature around 220°C and thermal stability without significant weight loss up to 400 °C under nitrogen or air atmosphere. The Nernst equation method was used to explore the number of electrons transferred at each oxidation step of the targeted two monomers. Furthermore, these two anodic electrochromic PESs were introduced into electrochromic devices accompanied with cathodic heptyl viologen (HV), and the resulted devices demonstrated a high coloration contrast and excellent electrochemical stability.

1. Introduction

Electrochromics are generally categorized as materials that undergo reversible color change under an applied electric field. Electrochromic (EC) materials are comprised of redox-active moieties that exhibit significant color changes and the transparency upon electrochemical reduction or oxidation process. Since Platt discovered the EC phenomenon in 1961, [1] then Deb published the first sandwich-type electrochromic device (ECD) fabricated by using amorphous WO_3 thin film in 1969, [2] EC technology is still prospering from then on [3–5]. There is a large number of chemical species exhibiting EC properties, such as metal oxides, [6–8 coordination complexes, [9,10] viologens, [11–13] and conducting polymers [14,15]. Nowadays, a flood of EC materials were reported and applied widely in our daily life, such as color changing eyewear, smart windows, display and adaptive camouflages etc. [16–19].

Over the past few decades, arylamine-based EC materials have attracted significant interest owing to the multicolored electrochromism as well as electrochemical stability [20–22]. It is worth mentioning that polymers containing triphenylamine (TPA) units not only possess dramatic color changes during oxidation but also show excellent reversibility and outstanding stability, which make them suitable candidates as electrochromic materials for practical utilization [23–29].

The related studies of TPA and its derivatives have been conducted extensively [30], and by introducing methoxy group into TPA system at the *para* position of phenyl ring can effectively prevent the coupling reaction to form TPA dimer, thus effectively enhance the redox stability [31–33]. In addition, dimethylamino group can not only reveals stronger electron donating ability than methoxy group but also provide more oxidation site when attached into anodic TPA-based EC materials. The simplest and typical material with dimethylamino groups is *N,N,N',N'*-tetramethyl-1,4-phenylenediamine (TMPD), which has already been investigated as display applications for a long period of time [34–36]. EC films based on 4-(dimethylamino)triphenylamine-functionalized polyamides with high contrast ratio and rapid switching behavior have been successfully reported in 2008 [37]. Recently, two small molecular TPA derivatives with dimethylamino substituents, **NTPPA** and **NTPB,** have also successfully synthesized in our group for the application of electrofluorochromic devices [38].

Apart from high-performance polymers with TPA units like polyamides, [39–41] polyimides, [42,43] polybenzoxazines [44] and epoxies, [45,46] poly(ether sulfone)s (PESs), a category of thermo-

* Corresponding author at: Institute of Polymer Science and Engineering, National Taiwan University, No.1, Sec. 4, Roosevelt Rd., Taipei 10617, Taiwan.
E-mail address: gsliou@ntu.edu.tw (G.-S. Liou).

https://doi.org/10.1016/j.electacta.2020.137552
0013-4686/

plastic polymers with good thermal stability, strong corrosion resistance and excellent mechanical properties, are commonly used in many realms, such as aviation, aerospace, microelectronics, nanotechnology, filtration and so on [47,48]. In addition, amorphous PES films are also colorless with high transparency which is an important merit for the further optical applications [49]. Thus, a series of multi-colored EC arylamine-based aromatic polyethers with methoxy protecting groups have been prepared by our group that could reveal the multi-colored (with 1 to 3 oxidation stages) behavior by increasing the electroactive sites [50]. However, it is still difficult to obtain PES arylamine-based PESs with four or more electroactive sites due to the complex synthesis route. Therefore, in this work, we introduce the dimethylamino unit into PES to increase the electroactive site via the facile synthesis route.

Herein, by integrating two dimethylamino groups and silyl ether protecting groups into *N,N,N′,N′*-tetraphenyl-*p*-phenylenediamine (TPPA) and *N,N,N′,N′*-tetraphenylbenzidine (TPB) moieties, two novel EC materials with four electroactive nitrogen centers, **NTPPA-2Si** and **NTPB-2Si**, have been prepared in this study. The Nernst equation has been applied here to investigate the electrochemical behaviors of monomers during the oxidation process. The obtained TPA-based monomers with disilyl ether groups can further react with bis(4-fluorophenyl)sulfone to obtain two novel electroactive poly(ether sulfone)s, **NTPPA-PES** and **NTPB-PES**. These PESs are expected to have four electroactive sites that increases two more additional oxidation stages than the corresponding PESs without dimethylamino groups. In addition, the incorporation of ether linkage is also effective to enhance their solubility for preparing colorless polymer films with high transparency and the corresponding EC behaviors are described hereby.

2. Experimental section

2.1. Materials

Commercially available chemical reagents, including 4-bromophenol (Alfa), *tert*-butyldimethylsily chloride (ACROS), imidazole (ACROS), *N,N*-dimethyl-*p*-phenylenediamine (Alfa), tris(dibenzylideneacetone)dipalladium(0) ($Pd_2(dba)_3$) (ACROS), tri-*tert*-butylphosphine ($P(tBu)_3$) (Alfa), sodium *tert*-butoxide (NaOtBu) (ACROS), 1,4-bromobenzene (ACROS), 4,4′-dibromo-1,1′-biphenyl (ACROS), palladium (II) acetate ($Pd(OAc)_2$) (Lancaster), bis(4-fluorophenyl) sulfone (ACROS), and cesium fluoride (ACROS) were used as received. Tetra-n-butylammonium tetrafluoroborate ($TBABF_4$) was acquired by ion exchanged of saturated sodium tetrafluoroborate aqueous solution with saturated tetra-n-butylammonium bromide aqueous solution, and then recrystallized by ethyl acetate.

2.2. Monomer and polymer synthesis

2.2.1. *(4-Bromophenoxy)*-tert-*butyldimethylsilane (Br-Si)*

4-Bromophenol (30 g, 0.17 mol) was added into a 500 mL three-necked round-bottom flask and dissolved in 200 mL of dimethylformamide (DMF) under nitrogen atmosphere. Then, imidazole (14 g, 0.21 mol) and *tert*-butylchlorodimethylsilane (**Cl-TBDMS**, 30 g, 0.20 mol) were added under 0 °C ice bath. The reaction was stirred for 20 h and was slowly returned to room temperature. After that, the mixture was poured into cold water and extracted with hexane. The organic phase was washed with saturate $NaHCO_{3(aq)}$ two times and dried over anhydrous sodium sulfate ($MgSO_4$). The solvent was removed under reduced pressure on a rotary evaporator and then a vacuum pump to obtain 48 g of colorless liquid (96% yield). mp < room temperature. ^{1}H NMR (400 MHz, DMSO-d_6, δ, ppm): 7.38–7.36 (d, 2 H, H_a), 6.79–6.77 (d, 2 H, H_b), 0.92 (s, 9 H, H_d), 0.15 (s, 6 H, H_c).

2.2.2. N-*(4-((tert-butyldimethylsilyl)oxy)phenyl)*-N′,N′-*dimethylbenzene-1,4-diamine (NDPA-Si)*

Tris(dibenzylideneacetone)dipalladium(0) ($Pd_2(dba)_3$, 0.7361 g, 0.80 mmol) and tri-*tert*-butylphosphine ($P(tBu)_3$, 0.4 mL, 1.60 mmol) were added into a 250 mL round-bottom flask containing 100 mL anhydrous toluene in the glove box preferentially. After stirring at room temperature under nitrogen atmosphere for 20 min to undergo the ligand exchange, *N,N*-dimethyl-*p*-phenylenediamine (13.61 g, 0.10 mol) was added to the flask sequentially and stirred at 50 °C till the *N,N*-dimethyl-*p*-phenylenediamine dissolved completely. **Br-Si** (22.90 g, 0.08 mol) and sodium *tert*–butoxide (NaO*t*Bu, 10.00 g, 0.10 mol) were then added into the solution. The mixture was stirred at 90 °C for 17 h and then extracted with EA and water till the water layer was cleared. The organic layer was dried over $MgSO_4$ and rotary evaporator. The residual was purified by flash column chromatography and recrystallized from hexane/EA to obtain 20.1 g of pale orange crystal (73% yield), mp: 93–95 °C. ^{1}H NMR (400 MHz, DMSO–d_6, δ, ppm): 7.34 (s, 1 H, H_d), 6.91–6.89 (d, 2 H, H_e), 6.79–6.77 (d, 2 H, H_c), 6.70–6.65 (m, 4 H, H_{b+f}), 2.80 (s, 6 H, H_a), 0.94 (s, 9 H, H_h), 0.14 (s, 6 H, H_g). ^{13}C NMR (125 MHz, DMSO–d_6, δ, ppm): 147.2 (C_9), 145.4 (C_2), 139.8 (C_6), 134.3 (C_5), 120.2 (C_3), 119.7 (C_7), 116.3 (C_4) 114.1 (C_8), 41.0 (C_1), 25.6 (C_{12}), 17.9 (C_{11}).

2.2.3. N,N′-*(1,4-phenylene)bis(*N-*(4-((*tert-*butyldimethylsilyl)oxy)phenyl)*-N″,N″-*dimethylbenzene-1,4-diamine) (NTPPA-2Si)*

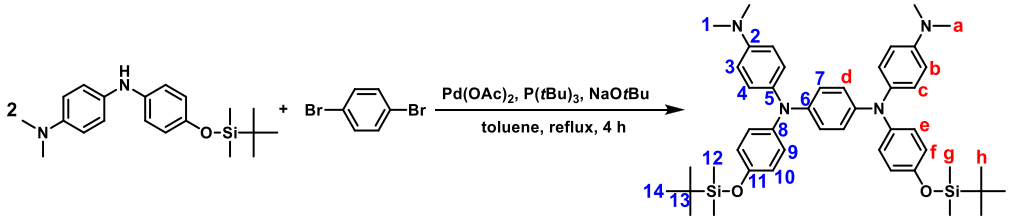

Palladium(II) acetate ($Pd(OAc)_2$, 130 mg, 0.58 mmol) and tri-*tert*-butylphosphine ($P(tBu)_3$, 0.13 mL, 0.54 mmol) were added into a 100 mL round-bottom flask containing 65 mL anhydrous toluene in the glove box preferentially. After stirring at room temperature under nitrogen atmosphere for 20 min to undergo the ligand exchange, 1,4-bromobenzene (3.42 g, 14.5 mmol), **NDPA-Si** (10.27 g, 30.0 mmol) and sodium *tert*–butoxide (NaO*t*Bu, 4.50 g, 46.8 mmol) were added into the container sequentially and then the solution was refluxed for 4 h. After cooling to room temperature, the mixture was extracted with water and dichloromethane till the water phase was cleared. The organic layer was dried over $MgSO_4$ and rotary evaporator. The residual was purified by column chromatography and then recrystallized by EA/MeOH to obtain 7.4 g of brown needle crystal (67% yield), mp: 165–167 °C. ^{1}H NMR (500 MHz, THF-d_8, δ, ppm): 6.94–6.92 (d, 4 H, H_c), 6.88–6.86 (d, 4 H, H_e), 6.77 (s, 4 H, H_d), 6.68–6.65 (t, 8 H, H_{b+f}), 2.88 (s, 12 H, H_a), 0.98 (s, 18 H, H_h), 0.18 (s, 12 H, H_g). ^{13}C NMR (125 MHz, THF-d_8, δ, ppm):

151.3 (C_6), 148.5 (C_{11}), 143.8 (C_2), 143.8 (C_8), 139.1 (C_5), 127.3 (C_4), 125.0 (C_9) 123.8 (C_7), 121.1 (C_{10}), 114.6 (C_3), 41.2 (C_1), 26.3 (C_{14}), 19.0 (C_{13}).

2.2.4. N,N'-((1,1′-biphenyl)-4,4′-diyl)bis(N-(4-((tert-butyldimethylsilyl)oxy)phenyl)-N",N"-dimethylbenzene-1,4-diamine) (NTPB-2Si)

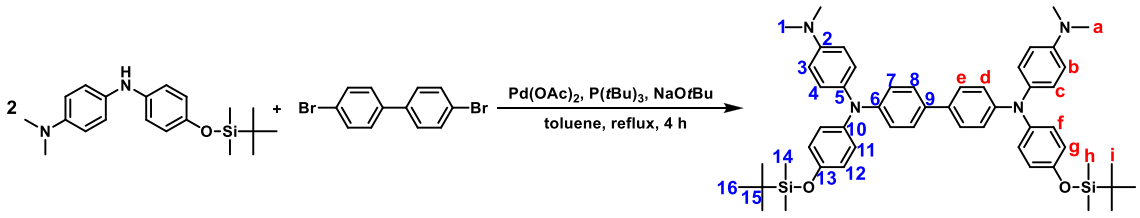

Palladium(II) acetate ($Pd(OAc)_2$, 130 mg, 0.58 mmol) and tri–*tert*-butylphosphine ($P(tBu)_3$, 0.13 mL, 0.54 mmol) were added into a 100 mL round-bottom flask containing 65 mL anhydrous toluene in the glove box preferentially. After stirring at room temperature under nitrogen atmosphere for 20 min to undergo the ligand exchange, 4,4′-dibromo-1,1′-biphenyl (4.52 g, 14.5 mmol), **NDPA-Si** (10.27 g, 30.0 mmol) and sodium *tert*–butoxide (NaO*t*Bu, 4.50 g, 46.8 mmol) were added into the container sequentially and then the solution was refluxed for 4 h. After cooling to room temperature, the mixture was extracted with water and dichloromethane till the water phase was cleared. The organic layer was dried over $MgSO_4$ and rotary evaporator. The residual was purified by column chromatography and then recrystallized by EA/DCM to obtain 9.5 g of yellow granular crystal (78% yield), mp: 178–181 °C. ^{1}H NMR (500 MHz, THF-d_8, δ, ppm): 7.33–7.31 (d, 4 H, H_e), 6.98–6.95 (m, 8 H, H_{c+f}), 6.90–6.89 (d, 4 H, H_d), 6.74–6.68 (m, 8 H, H_{b+g}), 2.90 (s, 12 H, H_a), 1.00 (s, 18 H, H_i), 0.20 (s, 12 H, H_h). ^{13}C NMR (125 MHz, THF-d_8, δ, ppm): 152.1 (C_6), 148.9 (C_5), 148.8 (C_{13}), 143.1 (C_2), 138.4 (C_{10}), 133.8 (C_9), 128.0 (C_4) 127.5 (C_8), 126.4 (C_{11}), 121.6 (C_7), 121.3 (C_{12}), 114.6 (C_3), 41.1 (C_1), 26.3 (C_{16}), 19.0 (C_{15}).

2.2.5. Preparation of NTPPA-PES and NTPB-PES poly(ether sulfone)s

CsF (0.35 g, 2.3 mmol) was added into a 50 mL two-necked round-bottom flask and dried at 150 °C for 3 h under the vacuum system. After cooling to the room temperature, **NTPPA-2Si** (0.76 g, 1.0 mmol) and 6.4 mL of anhydrous NMP were added into the flask and stirred at 120 °C for 3 h. After bis(4-fluorophenyl)sulfone (0.25 g, 1.0 mmol) was added into the reaction, the temperature was raised to 180 °C and stirred for 12 h. While the temperature returned to room temperature, the obtained polymer solution was slowly poured into methanol. The filtered was further purified by using Soxhlet extractor for 24 h. After that, the obtained **NTPPA-PES** was dried under vacuum system at 120 °C (Yield: 96%). **NTPB-PES** was also prepared by the same reaction condition.

2.3. Measurement

Melting point was mainly detected by OptiMelt-Automated Melting Point System at the scan rate of 5 °C/min and DSC at the scan rate of 5 °C/min if mentioned. ^{1}H NMR spectra were recorded on Bruker DPX-400NMR (400 MHz) and ^{13}C NMR was recorded on Bruker AVIII-500 MHz FT-NMR (125 MHz). The definition of splitting pattern is carried out as follows: s, singlet; d, doublet; t, triplet; q, quartet; m, multiplet. Fourier transform infrared (FT-IR) spectra were obtain by PerkinElmer Spectrum 100 Model FT-IR spectrometer. Electrochemistry was executed with CH Instrument 611B Electrochemical Analyzer or CH Instrument 612C Electrochemical Analyzer. Ultraviolet–visible (UV–Vis) spectra were carried out by Agilent 8453 UV–visible Spectroscopy System. CIELAB data were collected from JASCO V-650 UV–VIS spectrophotometer. Cyclic voltammetry was conducted by using the optically transparent thin layer electrochemical (OTTLE) cell (platinum gauze, 80 mesh, as working electrode; platinum wire as an auxiliary electrode; Ag/AgCl, 0.3 M KCl as a reference electrode) or two-electrode device with 20 mm × 20 mm working area at the scan rate of 50 mV/s. Differential pulse voltammetry was conducted with the same system at the scan rate of 2 mV/s, pulse amplitude of 50 mV, pulse width of 25 ms and pulse period of 0.2 s. Spectroelectrochemistry was conducted with the same system at the range of 300 and 1100 nm. UV–vis spectra for the wavelength range of 300–1600 nm were recorded by Hitachi U-4100 UV–vis-NIR spectrophotometer. The inherent viscosity was specified with a Tamson TV-2000 viscometer at 30 °C at the concentration 0.5 g/dL. A Waters chromatography unit interfaced with a Waters 2410 refractive index detector was used to conduct gel permeation chromatographic (GPC) analysis. Two Waters 5 μm Styragel HR-2 and HR-4 columns (7.8 mm I. D. × 300 mm) were connected with NMP in series as the eluent at a flow rate of 0.5 mL/min at 40 °C and were calibrated with polystyrene standards.

2.4. Preparation of the films

400 µL solutions of PESs in *o*-dichlorobenzene (2 mg/1 c.c.) were casted onto the ITO-coated glass substrates (3 × 2.5 cm^2) and dried at room temperature for 6 h, and then 160 °C for 3 h under vacuum. Subsequently, the obtained ITO-coated glass was cut into the size of 3 × 0.7 cm^2 for further measurements or 2 × 2 cm^2 for fabrication of EC devices.

2.5. Spectroelectrochemical measurement

Spectroelectrochemical measurements were applied to investigate the preliminary optical behavior of the two EC materials, **NTPPA-2Si** and **NTPB-2Si**, respectively, carried out by an optically transparent thin-layer electrode (OTTLE) coupled with UV–vis-NIR spectroscopy. The OTTLE cell was placed in the optical path of light beam in the spectrophotometer, which allowed us to acquire electronic absorption spectra during electrochemical experiments in a 0.1 M $TBABF_4$/NMP solution with 1 mM of the targeted EC materials. Besides, these new EC polymer films (**NTPPA-PES** and **NTPB-PES**) were casted on the ITO-coated glass substrate as working electrode were investigated by UV–vis-NIR spectroscopy in dry acetonitrile (CH_3CN) containing 0.1 M of $TBABF_4$ as electrolyte under nitrogen atmosphere

2.6. Device fabrication

First, prepare the polymer films on ITO substrates according to the previous method and then erase the area over 2 × 2 cm^2 with chloroform. Thermoset adhesive was dispensed on the ITO glass by full-auto dispenser and a tiny hole would be retained. Another blank ITO glass was then pasted onto it and baked at 150 °C for two hours. The gap was controlled by dispersing glass ball with a grain size about 120 µm into the adhesive. The liquid-type electrolyte (~0.05 mL) was then injected into the device by using a

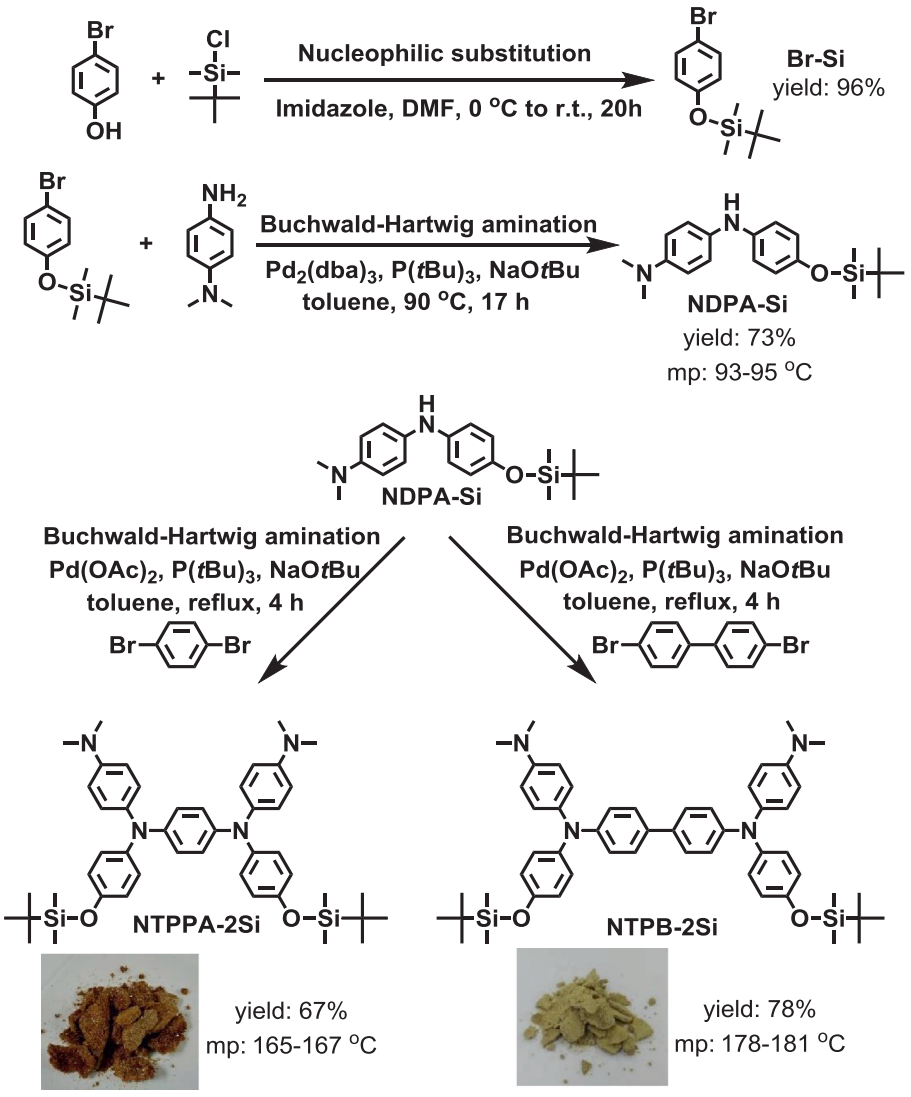

Scheme 1. Synthetic route of **NTPPA-2Si** and **NTPB-2Si**.

sample vacuum encapsulating system and the tiny hole would be filled up by UV gel. Stick copper tape on both side of the device for further measurement.

3. Results and discussion

3.1. Characterization of monomer

In order to obtain high molecular weight PESs with dimethylamino groups, the protecting silane unit as functional groups of monomers are necessary. Starting material (4-bromophenoxy)-*tert*-butyldimethylsilane (**Br-Si**), a high purity colorless liquid, was synthesized from 4-bromophenol with an equivalent of *tert*-dimethylsilyl chloride under base condition by the reported procedures [51]. *N*-(4-((*tert*-butyldimethylsilyl)oxy)phenyl)-*N*′,*N*′-dimethylbenzene-1,4-diamine (**NDPA-Si**), an important intermediate product, was prepared by Buchwald-Hartwig amination with a yield of 73%. Two novel final targeted monomers with silyl protecting groups, *N*,*N*′-(1,4-phenylene)bis(*N*-(4-((*tert*-butyldimethylsilyl)oxy)phenyl)-*N*″,*N*″-dimethylbenzene-1,4-diamine) (**NTPPA-2Si**) and *N*,*N*′-((1,1′-biphenyl)−4,4′-diyl)bis(*N*-(4-((*tert*-butyldimethylsilyl)oxy)phenyl)-*N*″,*N*″-dimethylbenzene-1,4-diamine) (**NTPB-2Si**), were synthesized from the similar procedure with the yield of 67% and 78%, respectively, as shown in Scheme 1. The synthesis and characterization of these compounds are illustrated in Supporting Information. Fourier transform infrared (FT-IR) spectra of the monomers were illustrated in **Fig. S1**, and the formation of **NTPPA-2Si** and **NTPB-2Si** could also be confirmed. Relative to **NDPA-Si**, the medium N–H stretching of secondary amine in the region of 3310–3350 cm^{-1} disappeared in the spectra of **NTPPA-2Si** and **NTPB-2Si**, and all the compounds showed similar characteristic bands such as the aliphatic C–H stretching at 2800–3000 cm^{-1}, the C–N stretching at 1252 cm^{-1} and the Si-C stretching at 823 cm^{-1}. The NMR spectra for the intermediate and two monomers were also measured and depicted in **Figs. S2**–**S13**. In addition, all the peaks related to the molecular structures could be assigned with the aid of two-dimensional (2D) COZY and HSQC NMR spectra. Thus, the results of all the spectroscopic analyses suggest the successful preparation of the targeted disilyl ether monomers.

3.2. Characterization of polymers

Two new types of PESs were prepared from the reaction of disilyl ether protecting groups of the multi-arylamine based monomers and bis(4-fluorophenyl)sulfone as shown in Scheme 2. During the polymerization process, the silyl protecting groups were deprotected by CsF to form phenoxide salts and further reacted

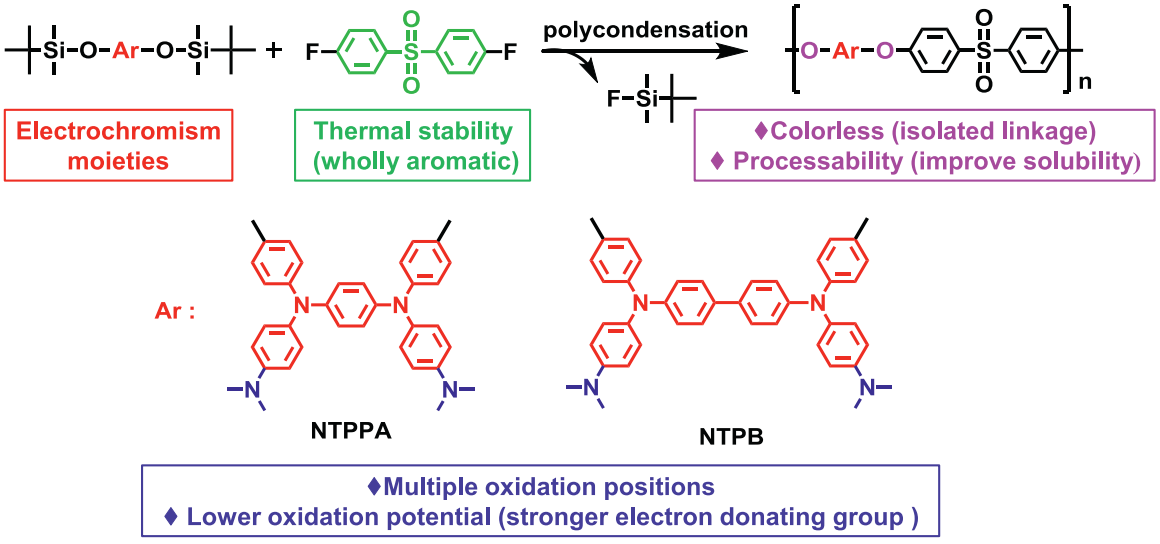

Scheme 2. Design concept and the relationship between structure and properties of the PESs.

with difluoride via nucleophilic substitution to produce PESs. This kind of method could avoid extra steps, such as pre-deprotection and purification of the resulted diphenols [52]. The results of all the spectroscopic analyses of FT-IR and ^{1}H NMR spectra for the PESs shown in **Figs. S14** and **S15** suggest the successful preparation of the target polymers.

The inherent viscosity and molecular weight of the obtained PESs are summarized in **Table S1**. The solubility behavior of the polymers listed in **Table S2** reveals high solubility in most organic solvents, such as NMP, DMAc, THF, $CHCl_3$ and *o*-DCB (*o*-dichlorobenzene) due to the bulky, packing-disruptive and three-dimensional propeller-like multi-arylamine units in the polymer backbone, indicating that these highly processable PESs should be suitable for solution-casting, spin-coating or inkjet-printing to afford high-performance thin films as potential candidates for optoelectronic devices applications.

The thermal properties of PESs were investigated by thermogravimetric analysis (TGA) (**Fig. S16**) and differential scanning calorimetry (DSC) (**Fig. S17**) and the results are summarized in **Table S3**. The prepared PESs with wholly aromatic structure exhibited high thermal stability without significant weight loss up to 400 °C under both nitrogen and air atmosphere, and the carbonized residues (char yields) in nitrogen atmosphere at 800 °C could reach to 45%. Furthermore, these PESs also possessed high glass-transition temperatures (T_g) of 220 and 226 °C for **NTPPA-PES** and **NTPB-PES**, respectively.

3.3. Electrochromic properties of the monomers

3.3.1. Electrochemical properties

The electrochemical properties of these two newly synthesized **TPA**-based EC monomers, **NTPPA-2Si** and **NTPB-2Si**, were investigated by differential pulse voltammetry (DPV). The measurements were conducted under an optically transparent thin-layer electrochemical (OTTLE) cell in anhydrous *N*-methyl-2-pyrrolidone (NMP) containing 1 mM of EC monomers and using 0.1 M of tetrabutylammonium tetrafluoroborate ($TBABF_4$) as the supporting electrolyte under nitrogen atmosphere. The resulted DPV diagrams for **NTPPA-2Si** and **NTPB-2Si** are depicted in **Figs. 1a** and **2a**. Since the aliphatic dimethylamine behaves stronger electron donating nature than aromatic amine, therefore, not only the oxidation potentials of the **NTPPA-2Si** and **NTPB-2Si** compounds at the first and second stages could be effectively reduced but also should exhibit four oxidation stages. However, oxidation potentials may be very close or even overlap as the result of symmetric and similar dimethylamino-containing TPA electroactive surroundings. Thence, the DPV diagram of **NTPPA-2Si** exhibited merely three major oxidation peaks at 0.46, 0.67 and 1.08 V together with EC coloring images from colorless at neutral state to green and then deep green at the semi-oxidation and fully oxidation stages, respectively, as shown in **Fig. 1**. In order to evaluate the electrochemical redox stability behaviors of the newly synthesized two monomers, optical recovery test from neutral to different oxidative stages of the monomers was conducted to confirm their electrochemical reversibility. Regardless of optical recovery in first and second oxidation stages, **NTPPA-2Si** could maintain excellent recovery up to 99.8% and 98.8%, respectively as depicted in **Fig. 1b** and **Fig. 1c**, respectively. On the contrary, **NTPB-2Si** with four theoretical electroactive sites revealed only two broader oxidation peaks at 0.60 V and 1.00 V maybe could be ascribed to the symmetric nitrogen centers of bis(diphenylamine)s linked via more distanced biphenyl than phenyl units as the bridge causing the more similar oxidation potentials to enhance the formation of one wave two electron oxidation process. **(Fig. 2a)**. The EC color change images of **NTPB-2Si** shown in **Fig. 2** from neutral colorless stage to green semi-oxidation, and then purple color fully oxidation stages together with excellent redox reversibility confirmed by the highly optical recovery ratio up to 98.5%.

3.3.2. Spectroelectrochemical properties

Both of the electroactive compounds were colorless in the neutral state (0 V). The spectra of absorption changes for **NTPPA-2Si** at different working potential are shown in **Fig. 1**. When the electroactive amino groups within **NTPPA-2Si** began to oxidize, a new shoulder peak at 430 nm and two other peaks centered at 744 and 1021 nm appeared simultaneously. According the results from DPV diagram shown in **Fig. 1a**, the first and second oxidation potential peaks were very close and even overlapped, implying that each electronic oxidation states may not be clearly determined. According to the observation of oxidation stage from 0 to 0.8 V, the first three electrons (will discuss later) exhibited the same tendency of absorption pattern as shown in **Fig. 1b**. Notably, the broad absorption peak at 1021 nm in the near-IR region within the range of 0–0.8 V could be classified as the intervalence charge transfer (IVCT) due to the coupling interaction of cation radicals between two electroactive amine *via* phenylene bridge [53]. The first ox-

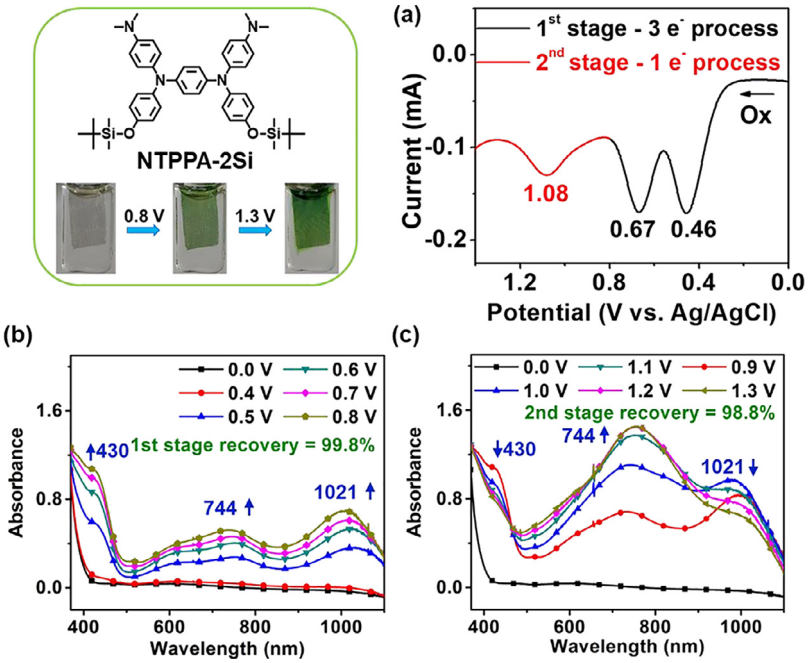

Fig. 1. (a) Differential pulse voltammetry diagram of **NTPPA-2Si**. Scan rate: 2 mV/s; pulse amplitude: 50 mV; pulse width: 25 ms; pulse period: 0.2 s. Absorbance spectra for **NTPPA-2Si** at the applied potential from (b) 0–0.8 V, (c) 0.9–1.3 V based on OTTLE. 0.6 μmol of **NTPPA-2Si** (1 mM) was dissolved in 0.6 ml NMP with 0.06 mmol (0.1 M) of $TBABF_4$ as the supporting electrolyte (V vs. Ag/AgCl).

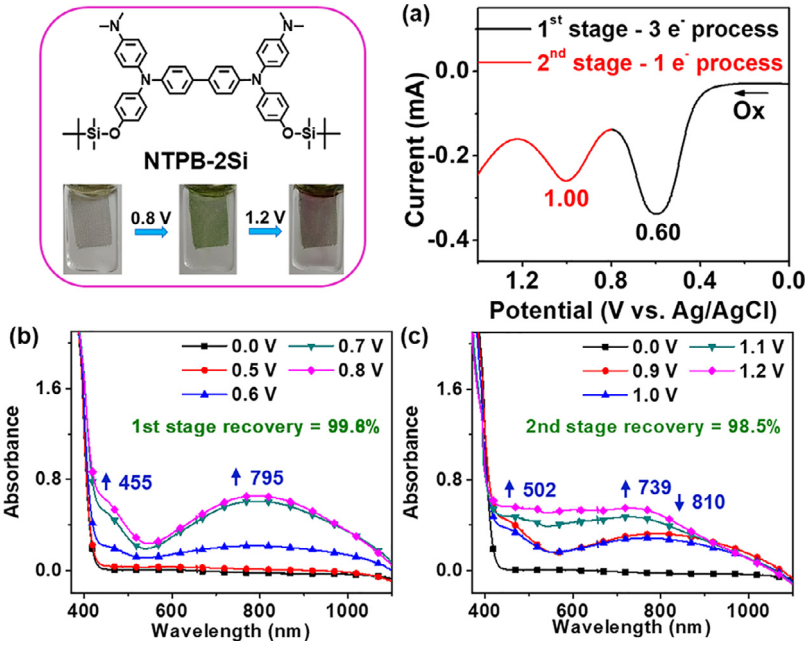

Fig. 2. (a) Differential pulse voltammetry diagram of **NTPB-2Si**. Scan rate: 2 mV/s; pulse amplitude: 50 mV; pulse width: 25 ms; pulse period: 0.2 s. Absorbance spectra for **NTPB-2Si** at the applied potential from (b) 0–0.8 V, (c) 0.9–1.2 V based on OTTLE. 0.6 μmol of **NTPB-2Si** (1 mM) was dissolved in 0.6 ml NMP with 0.06 mmol (0.1 M) of $TBABF_4$ as the supporting electrolyte (V vs. Ag/AgCl).

idation stage demonstrated extremely high reversibility of 99.8% based on the neutral form absorbance at 313 nm. As we applied a higher potential from 0.9 V to 1.3 V, **NTPPA-2Si** could reach the fully and final oxidation state of the fourth electron. The characteristic peaks ascribed to the first stage at 430 and 1021 nm would decrease while the new peak at 744 nm kept enhancing as shown in Fig. 1**c**. In the fourth and last oxidation state of **NTPPA-2Si**, the IVCT band in the near-IR region started to decay since all the four oxidation sites in the structure of **NTPPA-2Si** were completely oxidized, and the reversibility was 98.8% at this oxidation stage.

The DPV diagram of **NTPB-2Si** with biphenyl-linkage structure depicted in Fig. 2**a** exhibited only two broader peaks but not four or three peaks as the **NTPPA-2Si** with phenyl-linkage structure that may be attributed to the more extended biphenyl bridge between two diphenylamine units. Fig. 2**b** displays the spectroelectrochemical behavior of **NTPB-2Si** in the range of applied voltage 0–0.8 V, a shoulder peak at 455 and a broad absorption peak at 795 nm appeared simultaneously. At this applied voltage range, the first three oxidation centers (will discuss later) were oxidized with a reversibility of 99.6%. As the applied potential increased from 0.9 to 1.2 V, the remaining oxidation sites could then be oxidized as de-

Table 1
Results of Nernst equation method and DPV curves.

		$E_{applied}$ (V)[a]	fitting equation[b]	n[c]	Transferred e$^-$[d]
NTPPA-2Si	1st stage	0.4–0.48	$y = 0.0373x + 0.4337$	1.58	3
		0.5–0.6	$y = 0.0681x + 0.5026$	0.87	
		0.6–0.7	$y = 0.0960x + 0.5015$	0.61	
	2nd stage	0.96 −1.06	$y = 0.0521x + 0.9736$	1.13	1
NTPB-2Si	1st stage	0.5–0.6	$y = 0.0506x + 0.5420$	1.16	3
		0.62–0.7	$y = 0.0316x + 0.6183$	1.87	
	2nd stage	1.02 −1.1	$y = 0.0636x + 1.0208$	0.93	1

[a] Versus Ag/AgCl in NMP.
[b] Plot $E_{applied}$ vs $\log(A_0 - A_n)/(A_n - A_f)$ at the relative wavelength.
[c] Calculated from the slope of fitting equation and the Nernst equation value of 0.059.
[d] Amount of n electrons transferred for each stage.

picted in **Fig. 2c**, and the absorption peaks at 455 nm and 795 nm for the first oxidation stage decrease their intensity while the new flat and broad absorption between 502 and 739 nm became obvious with a reversibility of 98.5% at this second oxidation stage.

3.3.3. Nernst equation: exploring the number of electrons transferred at each oxidation stage

For the purpose of further exploring the actual situation of electronic oxidation at each step of **NTPPA-2Si** and **NTPB-2Si**, spectroelectrochemical spectra and Nernst equation were combined to investigate more detailed oxidation behaviors of the four redox-active sites within these two EC materials in this section [54–56], By utilizing the intensity change of characteristic absorption peak in spectroelectrochemical spectra derived from OTTLE measurement as the concentrations of electroactive compound at oxidation and neutral forms. The ratio of oxidized [*O*] and neutral forms [*N*], [*O*]/[*N*], at each different applied potential would be in accordance with the Nernst Eq. (1):

$$E_{applied} = E^0 + \frac{0.059}{n} log\left(\frac{[O]}{[N]}\right) \quad (1)$$

where $E_{applied}$ and E^0 represent the applied and standard potentials of redox reaction, respectively; [*O*] and [*N*] are the oxidized and neutral species, and 0.059 represents the ratio of the gas constant to the Faraday constant at room temperature. The [*O*]/[*N*] value could be calculated from absorbance changes measured by recording spectra after achieving equilibrium corresponding to each $E_{applied}$. In the equation, the measurement was performed at a gradually increasing applied potential; each applied potential was maintained until an equilibrium value of [*O*]/[*N*] was established in the entire thin layer solution contiguous to the platinum electrode by electrolysis and diffusion process. After obtaining the ratio of [*O*]/[*N*], plotting $E_{applied}$ to log([*O*]/[*N*]) by linear regression. The resulting slope value could be used to fit the coefficient of Nernst equation, and the resulted n value represented the number of electrons oxidized in the step [57,58].

The absorption spectral change for **NTPPA-2Si** and the corresponding Nernst equation plot depicted in **Fig. S18** and **Fig. S19**, respectively, was divided into three different voltage intervals **(a, b)** 0.4–0.48 V, **(c, d)** 0.5–0.6 V and **(e, f)** 0.6–0.7 V separately in **Fig. S18**. Since the oxidation potentials in this stage were close to form a broader peak, electrons were not oxidized one by one independently. To gain the fitting lines, the [*O*]/[*N*] values from different applied voltages at 750 nm was plotted with $E_{applied}$. Comparing the slope of fitting line in **Fig. S18b** (0.4–0.48 V) with the Nernstian value of 0.059 V, the obtained value $n_b = 1.58$. By using the same approaches, $n_d = 0.87$ and $n_f = 0.61$ could be also determined as shown in **Fig. S18d** and **Fig. S18f**. Through summing these n values ($n_b + n_d + n_f = 3.06$), the total number of electrons transferred was confirmed approximately to be 3. In other words, the applied voltage from 0.0 V to 0.8 V demonstrated three-electron transfer manifested by two waves oxidation process. Furthermore, when applying higher voltage interval to 0.96–1.06 V as shown in **Fig. S19**, the slope of the fitting line revealed one-electron transfer process ($n = 1.13$).

Similarly, for **NTPB-2Si** in **Fig. S20**, the study of Nernst equation demonstrated that **NTPB-2Si** undergoes the three-electrons oxidation process at applied potential from 0.5 to 0.7 V; and by using the same approach, $n_b = 0.93$ could be obtained at applied potential of 1.02–1.1 V for the one-electron oxidation process as shown in **Fig. S21.** These results derived from Nernst equation approach together with DPV diagrams are summarized in **Table 1**.

3.3.4. Electrochemical stability

The electrochemical stability of **NTPPA-2Si** and **NTPB-2Si** was examined by repetitive cyclic voltammetry (CV) test as shown in **Figs. 3** and **4**. Referring to DPV results, the CV tests were divided into three voltage stages up to 0.55 V, 0.8 V and 1.4 V for **NTPPA-2Si** and two stages up to 0.75 V and 1.4 V for **NTPB-2Si**, respectively, for continuous 100 cycles at the scan rate of 25 mV/s. And demonstrated that the former three electrons transfer oxidation at the oxidation stage with lower applied potentials exhibits extremely high electrochemical stability while the last stage at higher applied potential reveals less stable redox behaviors for both of the compounds. From the EC recovery tests of absorption spectra for these two compounds mentioned above in **Fig. 1b**, **1c** and **Fig. 2b**, **2c**, respectively, the results also demonstrated the same trend that these two EC compounds reveals excellent reversibility (>99.6%) at the first oxidation stage while decreases to 98.5% at the last stage.

3.4. Electrochromic properties of the polymers

3.4.1. Electrochemical properties

The electrochemical properties of the two new poly(ether sulfone)s, **NTPPA-PES** and **NTPB-PES**, were investigated by cyclic voltammetry with polymer thin films casted on the ITO-coated glass substrate as working electrode in the dry acetonitrile (CH_3CN) containing 0.1 M of $TBABF_4$ as an electrolyte under nitrogen atmosphere for oxidation measurements, and the results are summarized in **Fig. S22**. The oxidation potentials of **NTPPA-PES** showed four obvious oxidation peaks at 0.58, 0.68, 1.06 and 1.27 V, separately, for the four electroactive nitrogen centers in **Fig. S22a**. Although **NTPB-PES** also has four electroactive nitrogen centers as **NTPPA-PES**, while the oxidation behavior was different as depicted in **Fig. S22b** that the first oxidation peak at 0.69 V should be two-electron process contributed from subsequent dimethylamine groups, and the second oxidation peak at 1.22 V also exhibited two-electron process derived from tetraphenyl-benzidine (TPB) unit.

3.4.2. Spectroelectrochemical properties

According to the four electroactive nitrogen centers from dimethylamine and arylamine units, the EC process was divided

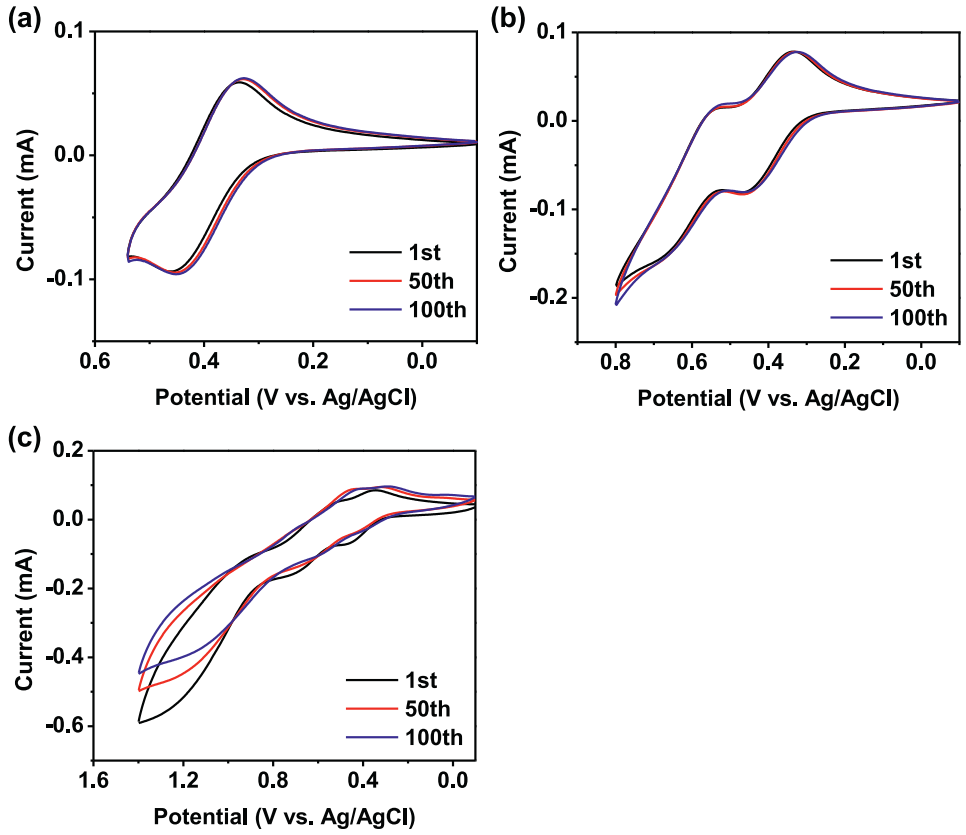

Fig. 3. Repetitive cyclic voltammetric diagrams at three different voltage ranges (a) −0.1–0.55 V, (b) −0.1–0.8 V, (c) −0.1–1.4 V (V vs. Ag/AgCl) of **NTPPA-2Si** (1 mM) dissolved in NMP with 0.1 M of $TBABF_4$ based on OTTLE at the scan rate of 25 mV/s.

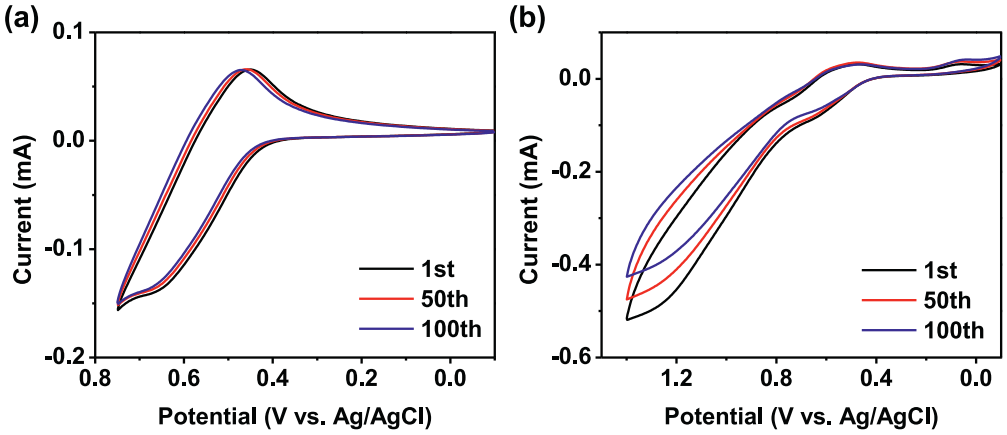

Fig. 4. Repetitive cyclic voltammetric diagrams at two different voltage ranges (a) −0.1–0.75 V, (b) −0.1–1.4 V (V vs. Ag/AgCl) of **NTPB-2Si** (1 mM) dissolved in NMP with 0.1 M of $TBABF_4$ based on OTTLE at the scan rate of 25 mV/s.

into four steps. For **NTPPA-PES**, when the applied potentials increased positively from 0 to 0.6 V, the characteristic absorption peak of neutral state at 322 nm decreased gradually while a new wide range absorption band with three peaks grew up at 600, 845 and 1049 nm during the first electron oxidation (Fig. 5**a**). As the potential was further increased to 0.7 V, all of the absorption peaks belonged to the first oxidation state reduced their intensity, and the characteristic absorption around 400–500 nm maintained its shoulder intensity, resulting in color change from blue to pale blue at the second oxidation state (Fig. 5**b**). Comparing to the oxidizing ability of aromatic amine (TPA) unit, the aliphatic amine (NMe_2) moiety should possess stronger basicity which leads to have lower oxidation voltage. Therefore, the first two oxidation steps could be attributed to the dimethylamino groups [37,59]. The EC images and the CIELAB data of semi-oxidized state **NTPPA-PES** film at the first two redox steps as depicted in Fig. 5 show the color change from highly transparent neutral state (0 V, L*: 97.45, a*: 1.60, b*: 0.07) to a blue (0.6 V, L*: 69.11, a*: −25.16, b*: 0.97), and then to pale blue (0.7 V, L*: 89.16, a*: −7.61, b*: 13.30). As the applied potential increased further to the third oxidation step (0.8–1.0 V), the characteristic absorption of the typical arylamine characteristic absorption peak at 415 nm and another intense intervalence charge transfer (IV-CT) broad band at near IR region centered at 942 nm grew up accompanying with the color change to green (1.0 V, L*: 58.88, a*: −11.86, b*: 14.94) at the third oxidation step (Fig. 5**c**). The broad absorption at the near-IR region as-

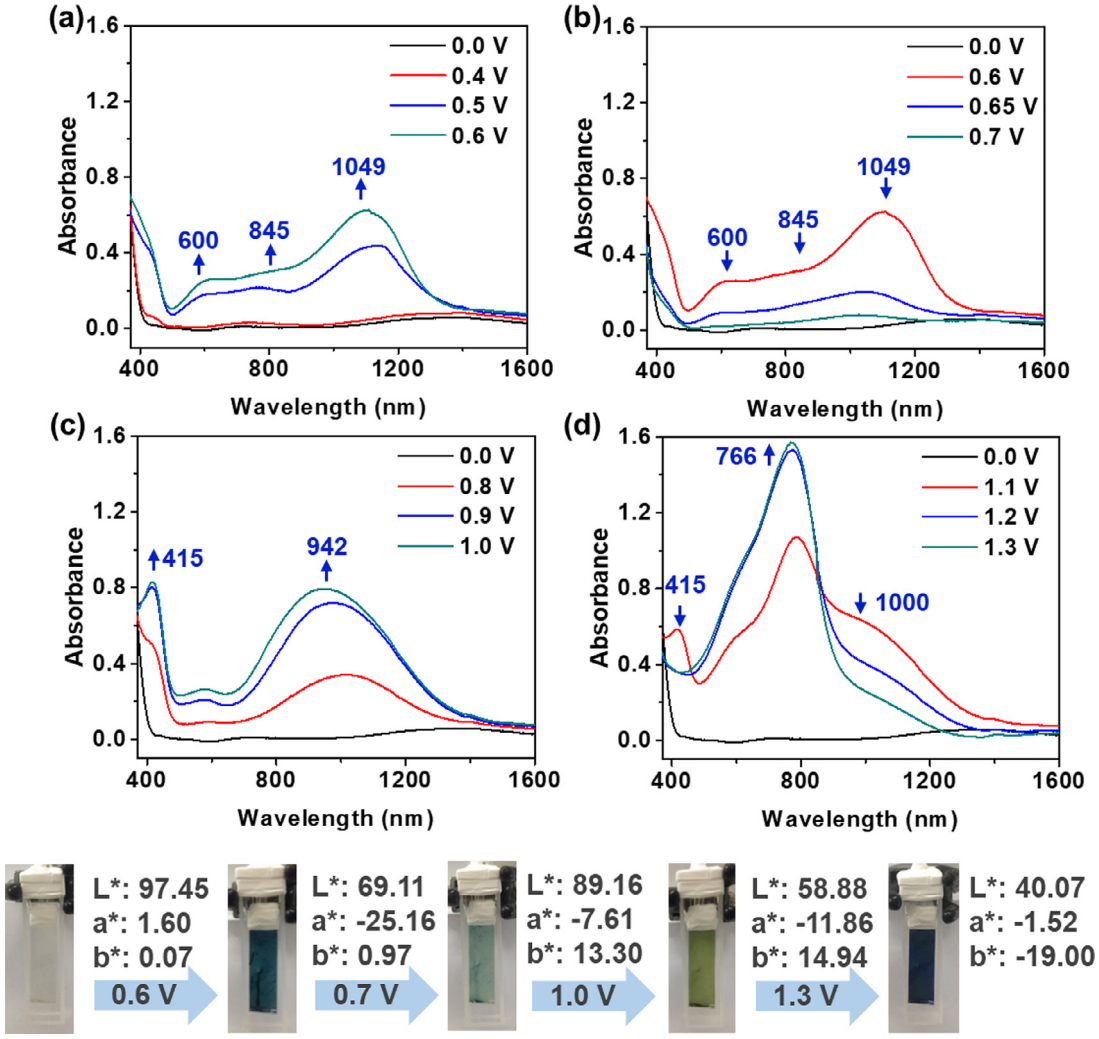

Fig. 5. Absorption spectra for (a) first, (b) second, (c) third and (d) fourth oxidation states of the **NTPPA-PES** film on the ITO-coated glass substrates in CH_3CN containing 0.1 M of $TBABF_4$ at the applied potential of (a) 0–0.6 V, (b) 0.6–0.7 V, (c) 0.8–1.0 V, (d) 1.1–1.3 V (V vs. Ag/AgCl) and the corresponding EC photographs. (For interpretation of the references to color in this figure, the reader is referred to the web version of this article.)

cribed to the IV-CT excitation caused by the electron coupling between neutral nitrogen and mono-cationic radical of TPA nitrogen centers in TPPA moiety via the phenyl bridge, which is consistent with the phenomenon classified by Robin and Day [52]. For the fully oxidation state at applied voltage (1.1–1.3 V), the two characteristic absorption peaks (415 nm, 942 nm) of the third oxidation state decreased, and a new sharp absorption peak at 766 nm appeared with a color change to dark blue (1.3 V, L*: 40.07, a*: −1.52, b*: −19.00) as shown in **Fig. 5d**. The reduced intensity of NIR absorption band demonstrated the further oxidation of mono-cationic radical species to the formation of dication in the TPPA segments. Subsequently, as the applied potential returned to 0 V, the film could recover to the original colorless neutral state.

NTPB-PES also could exhibit four stages of anodic color change by applying different related potentials. At the first stage from 0.0 to 0.6 V, the characteristic peak in the UV region decreased gradually while a broad peak centered at 760 nm grew up. The image of the EC film changed from colorless (0 V, L*: 99.90, a*: −0.07, b*: 3.34) to green (0.6 V, L*: 78.10, a*: −28.90, b*: 13.94) at first oxidation state (**Fig. 6a**). When the potential was set to 0.8 V, the characteristic absorption broad peak at 760 nm of the first oxidation state disappeared and the color would change back to almost colorless (0.8 V, L*: 98.47, a*: −4.61, b*: 17.07) at second oxidation state as shown in **Fig. 6b** after both electroactive sites of dimethylamino groups were oxidized to cation radicals. This decolorization behavior (disappearance of bands situated both in visible and NIR region) was similar to dimethylamine-substituted organic dyes, such as methylene blue and Rodamine B under electrochemical oxidation process [60]. For the third oxidation state from 0.9 to 1.0 V, two new typical oxidation characteristic absorption peaks at 485, 885, and a broad IV-CT band at 1380 nm od TPB moiety grew up with the color change to orange (1.0 V, L*: 58.83, a*: 14.44, b*: 55.74). When the applied voltage was adjusted to fully oxidation state (1.1–1.2 V), the two peaks at 485 and 1380 nm decreased, while a sharp and intensive peak at 833 nm arose rapidly with a strong color change from orange to dark blue (1.2 V, L*: 18.90, a*: −1.79, b*: −25.45) as shown in **Fig. 6d**. This **NTPB-PES** film also could recover to the same original colorless state as **NTPPA-PES** when the applied potential was released to 0 V. According to the results shown in **Fig. 5** and **Fig. 6**, these novel dimethylamino-substituted PESs demonstrated fascinating EC behaviors with relatively low applied voltage and multiple oxidation stages.

3.5. Device fabrication and EC properties

The two EC polymers were further introduced to fabricate electrochromic device (ECD) and the EC behaviors were systematically

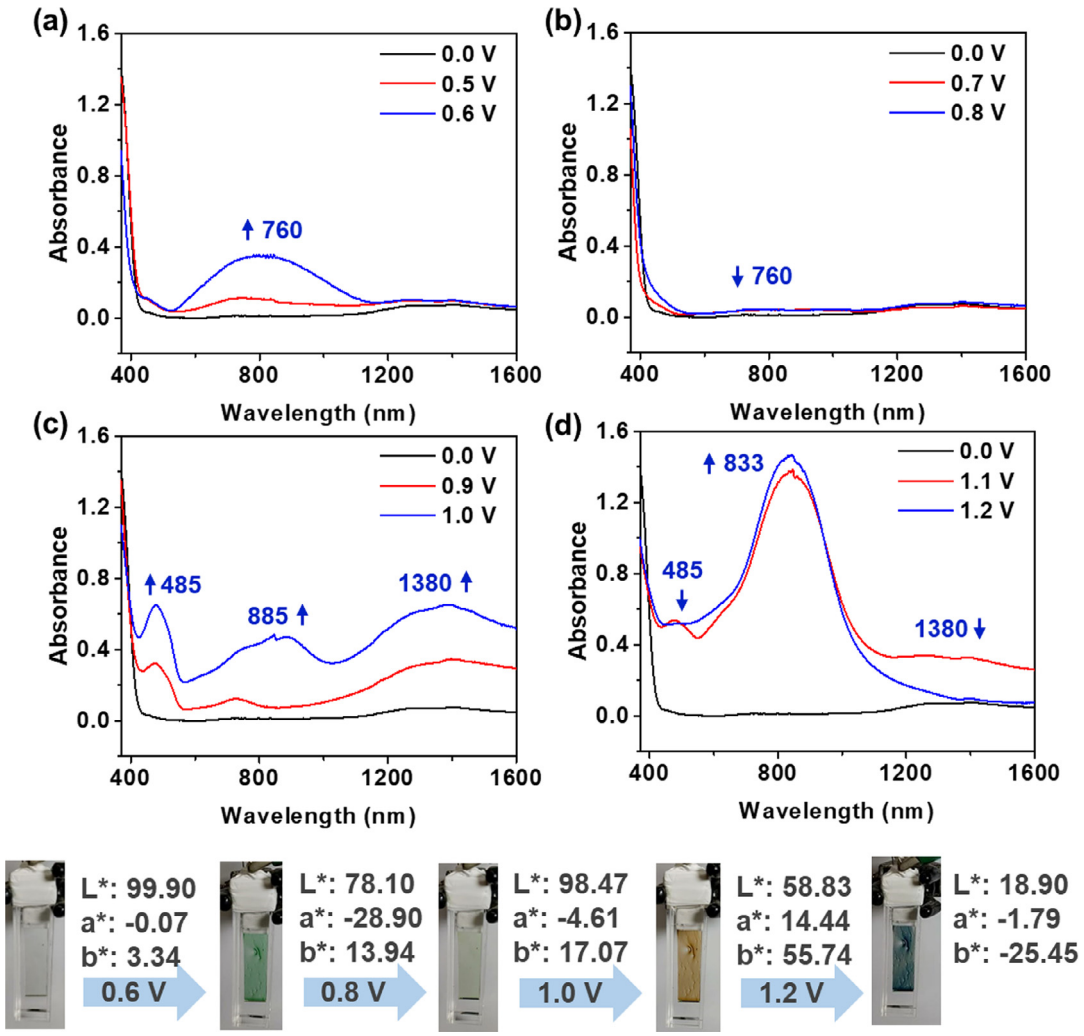

Fig. 6. Absorption spectra for (a) first, (b) second, (c) third and (d) fourth oxidation states of **NTPB-PES** film on the ITO-coated glass substrates in CH_3CN containing 0.1 M of $TBABF_4$ at the applied potential of (a) 0–0.6 V, (b) 0.7–0.8 V, (c) 0.9–1.0 V, (d) 1.1–1.2 V (V vs. Ag/AgCl) and the corresponding EC photographs. (For interpretation of the references to color in this figure, the reader is referred to the web version of this article.)

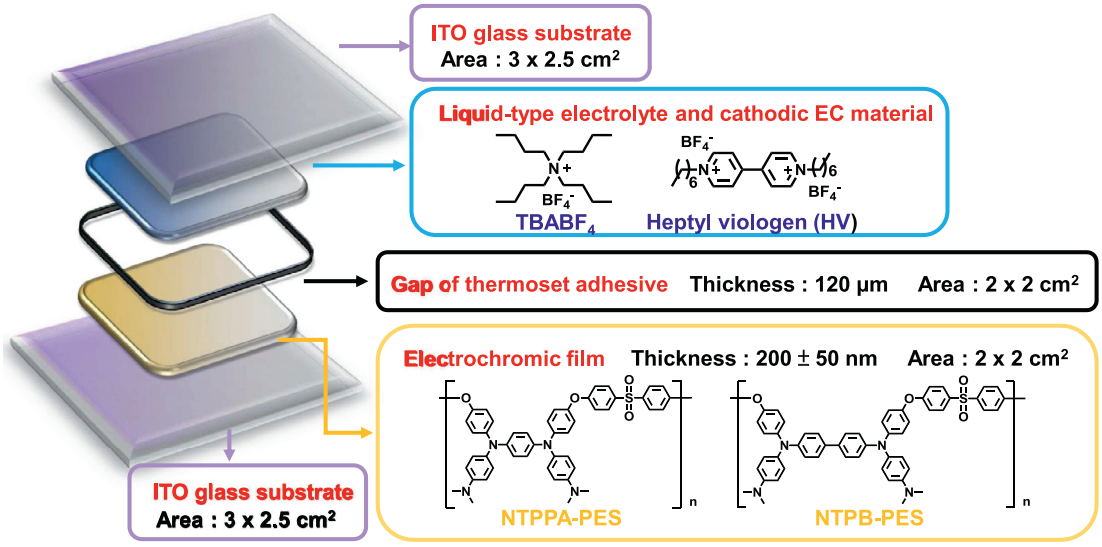

Fig. 7. Schematic diagram of the electrochromic device (ECD) based on these two PESs.

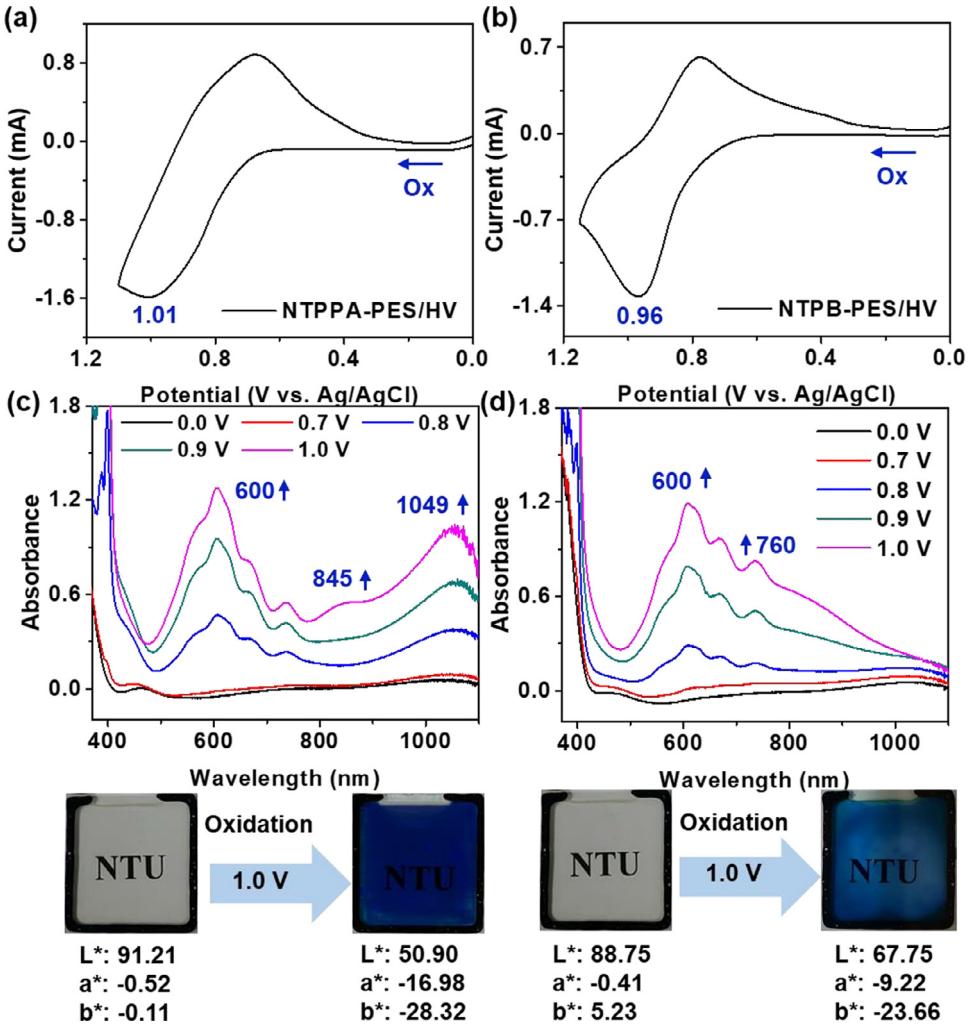

Fig. 8. Cyclic voltammograms of the ECDs for (a) **NTPPA-PES/HV** and (b) **NTPB-PES/HV** at a scan rate of 50 mV/s. Absorption spectra and the corresponding color changes of (c) **NTPPA-PES/HV** (d) **NTPB-PES/HV** based ECDs at the applied potential from 0 to 1.0 V with 2 cm × 2 cm active area containing 0.015 M of HV and 0.1 M of $TBABF_4$ as the supporting electrolyte in 0.05 mL PC (polymer film 200 ± 40 nm in thickness).

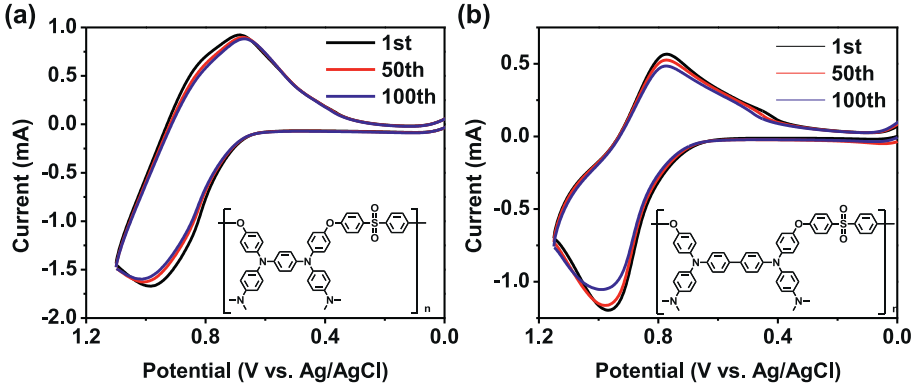

Fig. 9. Repetitive cyclic voltammograms (scan rate: 50 mV/s) of (a) **NTPPA-PES/HV** and (b) **NTPB-PBS/HV** ECD for 100 cycles. Device is ITO glasses with 2 cm × 2 cm active area containing 0.015 M of HV in about 0.05 mL PC with 0.1 M of TBABF4 as the supporting electrolyte (polymer film 200 ± 40 nm in thickness).

investigated. The procedure of preparing ECD is illustrated in **Fig. S23** and the schematic diagram of the devices is depicted in Fig. 7. In addition, cathodic EC material, heptyl viologen (HV), was introduced into the device as complementary EC material for building ambipolar system that not only could balance the charge of electroactive species to reduce the driving redox voltage but also efficaciously increase totally electrolyte concentration.

The spectroelectrochemical behaviors of ECDs based on **NTPPA-PES** and **NTPB-PES** without/with **HV** are summarized in **Fig. S24–S27**. The EC spectra changes of the prepared ECDs at the four oxidation stages were in accordance with those of original polymer films but higher applied voltage would be required in the device because of lower diffusion rate between electrode and ions from the electrolyte. Taking **NTPPA-PES** based ECD as example**,** the ap-

plied voltage required for the four oxidation stages were 2.3, 2.4, 2.6, 2.8 V (without **HV**) and 1.0, 1.5, 1.8, 2.0 V (with **HV**), respectively. It is worth noting that the PES film coupled with HV as ambipolar device system could effectively reduce driving voltage due to the complementary effect.

The electrochemical, spectroelectrochemical and the corresponding EC coloring behaviors of the ECDs derived from **NTPPA-PES/HV** and **NTPB-PES/HV** at the first oxidation state are depicted in **Fig. 8**. The oxidation potential peaks obtained by CV were 1.01 and 0.96 V for **NTPPA-PES/HV** and **NTPB-PBS/HV** as shown in **Fig. 8a** and **8b**, respectively. The EC behaviors and color changes of the devices at different working potentials from 0 to 1.0 V are demonstrated in **Fig. 8c** and **8d**. For **NTPPA-PES/HV** (**Fig. 8c**), three absorption peaks at 600, 845, and 1049 nm appeared with color change from colorless (0 V, L*: 91.21, a*: −0.52, b*: −0.11) to navy blue (1.0 V, L*: 50.90, a*: −16.98, b*: −28.32) at the first oxidation state. In the case of **NTPB-PBS/HV** (**Fig. 8d**), two absorption peaks emerged at 600 and 760 nm, and color changed from colorless (0 V, L*: 88.75, a*: −0.41, b*: 5.23) to blue (1.0 V, L*: 67.75, a*: −9.22, b*: −23.66) at the first oxidation state. The absorption peak at 600 nm could be ascribed to the contribution from the reduction of HV both in **NTPPA-PES/HV** and **NTPB-PBS/HV** ECDs. In addition, the long-term electrochemical stability of these two ECDs were also confirmed by repetitive cyclic voltammograms as shown in **Fig. 9.** After 100 cycles of continuous repeated redox scanning, both **NTPPA-PES/HV** and **NTPB-PBS/HV** devices still revealed excellent EC behaviors and excellent cyclic electrochemical stability.

4. Conclusion

Two novel dimethylamine-containing TPA-based EC materials with silyl functional groups, **NTPPA-2Si** and **NTPB-2Si**, were readily prepared by Buchwald-Hartwig amination and then go through a silyl polycondensation to synthesize two poly(ether sulfone)s (PESs), **NTPPA-PES** and **NTPB-PES**, respectively. The dimethylamino substituents not only provide stronger electron-donating ability to reduce oxidation potentials but also reveal multiple coloring stages comparing to their corresponding multi-arylamine structures without dimethylamino substituents. According to the results from the spectroelectrochemical spectra combining with Nernst equation, the numbers of multi-electrons transfer behaviors of the redox-active monomeric compounds during oxidation procedure could be determined. The obtained polymer films demonstrated fascinating four EC coloring-stage changes at relatively lower voltages. The ECDs derived from these anodic materials accompanying with cathodic HV exhibited high EC stability implying great potential for optoelectronic applications.

Authorship contribution statement

G.S.L and C.L.H conceived the study project. G.S.L guided and supervised the project. C.L.H fabricated the devices and performed the measurements. C.L.H, Y.R.K and Y.J.S wrote the first draft of the manuscript. G.S.L revised the manuscript.

Declaration of Competing Interest

The authors declare that they have no known competing financial interests or personal relationships that could have appeared to influence the work reported in this paper.

Acknowledgements

This work was financially supported by the “Advanced Research Center for Green Materials Science and Technology” from The Featured Area Research Center Program within the framework of the Higher Education Sprout Project by the Ministry of Education in Taiwan (109L9006) and the Ministry of Science and Technology in Taiwan (MOST 109-2634-F-002-042, 107-2113-M-002-024-MY3, and 107-2221-E-002-066-MY3).

Supplementary materials

Supplementary material associated with this article can be found, in the online version, at doi:10.1016/j.electacta.2020.137552.

References

[1] J.R. Platt, A possible change of color producible in dyes by an electric field, J. Chem. Phys. 34 (1961) 862–863.
[2] S.K. Deb, A novel electrophotographic system, Appl. Opt. 8 (1969) 192–195.
[3] H.N. Hersh, W.E. Kramer, J.H. McGee, Mechanism of electrochromism in WO_3, Appl. Phys. Lett. 27 (1975) 646–648.
[4] R.J. Colton, A.M. Guzman, J.W. Rabalais, Electrochromism in some thin-film transition-metal oxides characterized by x-ray electron spectroscopy, J. Appl. Phys. 49 (1978) 409–416.
[5] S. Gottesfeld, J. Electrochem, Electrochromism in anodic iridium oxide films: II. pH effects on corrosion stability and the mechanism of coloration and bleaching, J. Electrochem. Soc. 126 (1979) 742–750.
[6] N.R. de Tacconi, K. Rajeshwar, R.O. Lezna, Metal hexacyanoferrates: electrosynthesis, in situ characterization, and applications, Chem. Mater. 15 (2003) 3046–3062.
[7] A. Ghicov, M. Yamamoto, P. Schmuki, Lattice widening in niobium-doped TiO_2 Nanotubes: efficient ion intercalation and swift electrochromic contrast, Angew. Chem. Int. Ed. 47 (2008) 7934–7937.
[8] D. Qiu, H. Ji, X. Zhang, H. Zhang, H. Cao, G. Chen, T. Tian, Z. Chen, X. Guo, L. Liang, J. Gao, F. Zhuge, Electrochromism of nanocrystal-in-glass tungsten oxide thin films under various conduction cations, Inorg. Chem. 58 (2019) 2089–2098.
[9] R.J. Mortimer, Electrochromic materials, Chem. Soc. Rev. 26 (1997) 147–156.
[10] N.L. Bill, O. Trukhina, J.L. Sessler, T. Torres, Supramolecular electron transfer--based switching involving pyrrolic macrocycles. A new approach to sensor development? Chem. Commun. 51 (2015) 7781–7794.
[11] N.M. Rowley, R.J. Mortimer, New electrochromic materials, Sci. Prog. 85 (2002) 243–262.
[12] C.L. Bird, Electrochemistry of the viologens, Chem. Soc. Rev. 10 (1981) 49–82.
[13] K. Madasamy, D. Velayutham, V. Suryanarayanan, M. Kathiresan, K.-C. Ho, Viologen-based electrochromic materials and devices, J. Mater. Chem. C. 7 (2019) 4622–4637.
[14] C.M. Amb, A.L. Dyer, J.R. Reynolds, Navigating the color palette of solution-processable electrochromic polymers, Chem. Mater. 23 (2011) 397–415.
[15] J.A. Kerszulis, C.M. Amb, A.L. Dyer, J.R. Reynolds, Follow the yellow brick road: structural optimization of vibrant yellow-to-transmissive electrochromic conjugated polymers, Macromolecules 47 (2014) 5462–5469.
[16] A.M. Österholm, D.E. Shen, J.A. Kerszulis, R.H. Bulloch, M. Kuepfert, A.L. Dyer, J.R. Reynolds, Four shades of brown: tuning of electrochromic polymer blends toward high-contrast eyewear, ACS Appl. Mater. Interfaces. 7 (2015) 1413–1421.
[17] C.G. Granqvist, M.A. Arvizu, İ.B. Pehlivan, H.Y. Qu, R.T. Wen, G.A. Niklasson, Electrochromic materials and devices for energy efficiency and human comfort in buildings: a critical review, Electrochim. Acta. 259 (2018) 1170–1182.
[18] S. Beaupré, A.-C. Breton, J. Dumas, M. Leclerc, Multicolored electrochromic cells based on poly (2, 7-carbazole) derivatives for adaptive camouflage, Chem. Mater. 21 (2009) 1504–1513.
[19] J. Kim, M. Rémond, D. Kim, H. Jang, E. Kim, Electrochromic conjugated polymers for multifunctional smart windows with integrative functionalities, Adv. Mater. Technol. (2020) 1900890.
[20] L. Otero, L. Sereno, F. Fungo, Y.-L. Liao, C.-Y. Lin, K.-T. Wong, Synthesis and properties of a novel electrochromic polymer obtained from the electropolymerization of a 9,9′-Spirobifluorene-Bridged Donor−Acceptor (D−A) Bichromophore System, Chem. Mater. 18 (2006) 3495–3502.
[21] J. Natera, L. Otero, L. Sereno, F. Fungo, N.-S. Wang, Y.-M. Tsai, T.-Y. Hwu, K.-T. Wong, A novel electrochromic polymer synthesized through electropolymerization of a new donor− acceptor bipolar system, Macromolecules 40 (2007) 4456–4463.
[22] Z. Ning, H. Tian, Triarylamine: a promising core unit for efficient photovoltaic materials, Chem. Commun. 37 (2009) 5483–5495.
[23] M. h. Chahma, J.B. Gilroy, R.G. Hicks, Linear and branched electroactive polymers based on ethylenedioxythiophene–triarylamine conjugates, J. Mater. Chem. 17 (2007) 4768–4771.
[24] S.-H. Cheng, S.-H. Hsiao, T.-H. Su, G.-S. Liou, Novel aromatic poly (amine-imide) s bearing a pendent triphenylamine group: synthesis, thermal, photophysical, electrochemical, and electrochromic characteristics, Macromolecules 38 (2005) 307–316.
[25] C.-W. Chang, G.-S. Liou, Novel anodic electrochromic aromatic polyamides with multi-stage oxidative coloring based on N, N, N′, N′-tetraphenyl-p-phenylenediamine derivatives, J. Mater. Chem. 18 (2008) 5638–5646.

[26] P. Blanchard, C. Malacrida, C. Cabanetos, J. Roncali, S. Ludwigs, Triphenylamine and some of its derivatives as versatile building blocks for organic electronic applications, Polym. Int. 68 (2019) 589–606.
[27] Y. Dai, W. Li, Z. Chen, X. Zhu, J. Liu, R. Zhao, D.S. Wright, A. Noori, M.F. Mousavi, C. Zhang, An air-stable electrochromic conjugated microporous polymer as an emerging electrode material for hybrid energy storage systems, J. Mater. Chem. A. 7 (2019) 16397–16405.
[28] J. Zeng, H. Li, Z. Wan, L. Ai, P. Liu, W. Deng, Colorless-to-black electrochromic materials and solid-state devices with high optical contrast based on cross-linked Poly (4-vinyltriphenylamine), Sol. Energy Mater. Sol. Cells. 195 (2019) 89–98.
[29] H.-J. Yen, G.-S. Liou, Solution-processable novel near-infrared electrochromic aromatic polyamides based on electroactive Tetraphenyl-p-Phenylenediamine moieties, Chem. Mater. 21 (2009) 4026–4070.
[30] H.-J. Yen, G.-S. Liou, Design and preparation of triphenylamine-based polymeric materials towards emergent optoelectronic applications, Prog. Polym. Sci. 89 (2019) 250–287.
[31] H.-J. Yen, H.-Y. Lin, G.-S. Liou, Novel starburst triarylamine-containing electroactive aramids with highly stable electrochromism in near-infrared and visible light regions, Chem. Mater. 23 (2011) 1874–1882.
[32] L.-C. Lin, H.-J. Yen, Y.-R. Kung, C.-M. Leu, T.-M. Lee, G.-S. Liou, Novel near-infrared and multi-colored electrochromic polybenzoxazines with electroactive triarylamine moieties, J. Mater. Chem. C. 2 (2014) 7796–7803.
[33] J.-T. Wu, T.-L. Hsiang, G.-S. Liou, Synthesis and optical properties of redox-active triphenylamine-based derivatives with methoxy protecting groups, J. Mater. Chem. C. 6 (2018) 13345–13351.
[34] N. Leventis, Characterization of 3× 3 matrix arrays of solution-phase electrochromic cells, J. Electrochem. Soc. 145 (1998) L55.
[35] K.-C. Ho, Y.-W. Fang, Y.-C. Hsu, L.-C. Chen, The influences of operating voltage and cell gap on the performance of a solution-phase electrochromic device containing HV and TMPD, Solid State Ionics 165 (2003) 279–287.
[36] D. Weng, Y. Shi, J. Zheng, C. Xu, High performance black-to-transmissive electrochromic device with panchromatic absorption based on TiO2-supported viologen and triphenylamine derivatives, Org. Electron. 34 (2016) 139–145.
[37] S.-H. Hsiao, G.-S. Liou, Y.-C. Kung, H.-J. Yen, High contrast ratio and rapid switching electrochromic polymeric films based on 4-(dimethylamino) triphenylamine-functionalized aromatic polyamides, Macromolecules 41 (2008) 2800–2808.
[38] J.-T. Wu, H.-T. Lin, G.-S. Liou, Synthesis and characterization of novel triarylamine derivatives with dimethylamino substituents for application in optoelectronic devices, ACS Appl. Mater. Interfaces. 11 (2019) 14902–14908.
[39] L.-T. Huang, H.-J. Yen, J.-H. Wu, G.-S. Liou, Preparation and characterization of near-infrared and multi-colored electrochromic aramids based on aniline-derivatives, Org. Electron. 13 (2012) 840–849.
[40] H.-S. Liu, B.-C. Pan, D.-C. Huang, Y.-R. Kung, C.-M. Leu, G.-S. Liou, Highly transparent to truly black electrochromic devices based on an ambipolar system of polyamides and viologen, NPG Asia Mater. 9 (2017) e388 -e388.
[41] N. Sun, K. Su, Z. Zhou, X. Tian, Z. Jianhua, D. Chao, D. Wang, F. Lissel, X. Zhao, C. Chen, High-performance emission/color dual-switchable polymer-bearing pendant tetraphenylethylene (TPE) and triphenylamine (TPA) moieties, Macromolecules 52 (2019) 5131–5139.
[42] H.-J. Yen, C.-J. Chen, G.-S. Liou, Flexible multi-colored electrochromic and volatile polymer memory devices derived from starburst triarylamine-based electroactive polyimide, Adv. Funct. Mater. 23 (2013) 5307–5316.
[43] H.-J. Yen, J.-H. Wu, Y.-H. Huang, W.-C. Wang, K.-R. Lee, G.-S. Liou, Novel thermally stable and soluble triarylamine functionalized polyimides for gas separation, Polym. Chem. 5 (2014) 4219–4226.
[44] L.-C. Lin, H.-J. Yen, C.-J. Chen, C.-L. Tsai, G.-S. Liou, Novel triarylamine-based polybenzoxazines with a donor–acceptor system for polymeric memory devices, Chem. Commun. 50 (2014) 13917–13920.
[45] Y.-W. Chuang, H.-J. Yen, G.-S. Liou, A facile approach to multicolored electrochromic triarylamine-based thermoset epoxy materials with tunable intervalence charge transfer behavior, Chem. Commun. 49 (2013) 9812–9814.
[46] Y.-W. Chuang, H.-J. Yen, J.-H. Wu, G.-S. Liou, Colorless triphenylamine-based aliphatic thermoset epoxy for multicolored and near-infrared electrochromic applications, ACS Appl. Mater. Interfaces. 6 (2014) 3594–3599.
[47] M.A. Hickner, H. Ghassemi, Y.S. Kim, B.R. Einsla, J.E. McGrath, Alternative polymer systems for proton exchange membranes (PEMs), Chem. Rev. 104 (2004) 4587–4612.
[48] F. Li, J. Wang, M. Zhou, X. Liu, C. Wang, D. Chao, Synthesis and electrochemical properties of a novel poly (ether sulfone) with oligoaniline pendants, Chem. Res. Chin. Univ. 31 (2015) 1066–1071.
[49] H.R. Kricheldorf, K. Bornhorst, Syntheses of multicyclic poly (ether sulfone) s from 5,5′, 6,6′-tetrahydroxy-3,3,3′,3′-tetramethyl spirobisindane and 4,4′;-bis (4-chlorophenyl) sulfones, J. Polym. Sci., Part A: Polym. Chem. 46 (2008) 3732–3739.
[50] J.-T. Wu, Y.-Z. Fan, G.-S. Liou, Synthesis, characterization and electrochromic properties of novel redox triarylamine-based aromatic polyethers with methoxy protecting groups, Polym. Chem. 10 (2019) 345–350.
[51] J.T.W. Kan, P. Toy, Poly (ethylene glycol)-supported α, α, α-trifluoroacetophenone in dioxirane mediated alkene epoxidation reactions, Tetrahedron Lett. 45 (2004) 6357–6359.
[52] H.R. Kricheldorf, G. Bier, New polymer synthesis. IX. Synthesis of poly (ether sulfone) s from silylated diphenols or hydroxybenzoic acids, J. Polym. Sci. Polym. Chem. Ed. 21 (1983) 2283–2289.
[53] M.B. Robin, P. Day, Mixed valence chemistry-a survey and classification, Adv. Inorg. Chem. Radiochem. 10 (1968) 247–422.
[54] A.J. Bard, L.R. Faulkner, Electrochem. Methods: Fundamentals and Applications, Wiley, New York, 2001.
[55] E.T. Seo, R.F. Nelson, J.M. Fritsch, L.S. Marcoux, D.W. Leedy, R.N. Adams, On the α, α'Annelation of cyclic ketones, J. Am. Chem. Soc. 88 (1966) 3498–3503.
[56] R.R. Nelson, R.N. Adams, Anodic oxidation pathways of substituted triphenylamines. II. Quantitative studies of benzidine formation, J. Am. Chem. Soc. 90 (1968) 3925–3930.
[57] H.-J. Yen, S.-M. Guo, G.-S. Liou, J.-C. Chung, Y.-C. Liu, Y.-F. Lu, Y.-Z. Zeng, Mixed-valence class I transition and electrochemistry of bis (triphenylamine)-based aramids containing isolated ether-linkage, J. Polym. Sci. Part A: Polym. Chem. 49 (2011) 3805–3816.
[58] L.-T. Huang, H.-J. Yen, G.-S. Liou, Substituent effect on electrochemical and electrochromic behaviors of ambipolar aromatic polyimides based on aniline derivatives, Macromolecules 44 (2011) 9595–9610.
[59] S.-H. Hsiao, Y.-H. Hsiao, Y.-R. Kung, C.-M. Leu, T.-M. Lee, Triphenylamine-based redox-active aramids with 1-piperidinyl substituent as an auxiliary donor: enhanced electrochemical stability and electrochromic performance, React. Funct. Polym. 108 (2016) 54–62.
[60] N. Bensalah, A. Abdel-Wahab, Electrochemical Treatment of synthetic and actual dyeing wastewaters using BDD anodes, Air Soil Water Res. 3 (2010) 45–56.